Clinical Cancer Research

# Treatment Response Assessment in IDH-Mutant Glioma Patients by Noninvasive 3D Functional Spectroscopic Mapping of 2-Hydroxyglutarate

Ovidiu C. Andronesi[1], Franziska Loebel[1,2,3], Wolfgang Bogner[1,4], Małgorzata Marjańska[5], Matthew G. Vander Heiden[6], A. John Iafrate[7], Jorg Dietrich[8], Tracy T. Batchelor[8], Elizabeth R. Gerstner[8], William G. Kaelin[9], Andrew S. Chi[8], Bruce R. Rosen[1], and Daniel P. Cahill[2]

## Abstract

**Purpose:** Measurements of objective response rates are critical to evaluate new glioma therapies. The hallmark metabolic alteration in gliomas with mutant isocitrate dehydrogenase (IDH) is the overproduction of oncometabolite 2-hydroxyglutarate (2HG), which plays a key role in malignant transformation. 2HG represents an ideal biomarker to probe treatment response in IDH-mutant glioma patients, and we hypothesized a decrease in 2HG levels would be measureable by *in vivo* magnetic resonance spectroscopy (MRS) as a result of antitumor therapy.

**Experimental Design:** We report a prospective longitudinal imaging study performed in 25 IDH-mutant glioma patients receiving adjuvant radiation and chemotherapy. A newly developed 3D MRS imaging was used to noninvasively image 2HG. Paired Student *t* test was used to compare pre- and posttreatment tumor 2HG values. Test–retest measurements were performed to determine the threshold for 2HG functional spectroscopic maps (fSM). Univariate and multivariate regression were performed to correlate 2HG changes with Karnofsky performance score (KPS).

**Results:** We found that mean 2HG (2HG/Cre) levels decreased significantly (median = 48.1%; 95% confidence interval = 27.3%–56.5%; $P = 0.007$) in the posttreatment scan. The volume of decreased 2HG correlates ($R^2 = 0.88$, $P = 0.002$) with clinical status evaluated by KPS.

**Conclusions:** We demonstrate that dynamic measurements of 2HG are feasible by 3D fSM, and the decrease of 2HG levels can monitor treatment response in patients with IDH-mutant gliomas. Our results indicate that quantitative *in vivo* 2HG imaging may be used for precision medicine and early response assessment in clinical trials of therapies targeting IDH-mutant gliomas. *Clin Cancer Res; 22(7); 1632–41. ©2015 AACR.*



## Introduction

Intracranial malignant diffuse gliomas are a leading cause of cancer-related death in people under the age of 45 years. After initial diagnosis and therapy with surgery, radiation (1), and chemotherapy (2, 3), these diffusely infiltrative gliomas often regrow as malignant lesions, and then lack effective treatment, representing a substantial unmet clinical need. Indeed, the longitudinal treatment monitoring of diffuse gliomas with conventional MRI has been a substantial challenge, as radiochemotherapy induced alterations and treatment with antiangiogenic agents often result in treatment-related imaging changes on MRI that are difficult to distinguish from true disease progression (4, 5). Methods to discern tumor progression from treatment-associated changes (true/pseudo-progression/response) are urgently needed, particularly to measure objective response rates in clinical trials of novel glioma treatments.

A majority (50%–86%) of gliomas diagnosed in younger adults (<45 years old) have recurrent somatic mutations in the genes encoding $NADP^+$-dependent isocitrate dehydrogenase 1 and 2 (*IDH1*/*IDH2*; refs. 6, 7). These heterozygous mutations, characteristically nonsynonymous point mutations of Arginine at the 132 residue (R132) of the *IDH1* gene or the 172 residue (R172) of *IDH2*, result in a neomorphic gain of enzymatic function, leading to excess turnover of α-ketoglutarate (αKG, known as 2-oxoglutarate) and accumulation of the oncometabolite 2-hydroxyglutarate (2HG; ref. 8). Increased levels of 2HG inhibit αKG-dependent dioxygenases (9) and chromatin modifiers, promoting tumorigenesis through DNA/histone hypermethylation and genome-wide alterations in the epigenetic control of gene expression (10, 11).

[1]Athinoula A. Martinos Center for Biomedical Imaging, Department of Radiology, Massachusetts General Hospital, Harvard Medical School, Boston, Massachusetts. [2]Department of Neurosurgery, Massachusetts General Hospital, Harvard Medical School, Boston, Massachusetts. [3]Department of Neurosurgery, Charité Medical University, Berlin, Germany. [4]High Field MR Center, Department of Biomedical Imaging and Image-guided Therapy, Medical University Vienna, 1090 Vienna, Austria. [5]Center for Magnetic Resonance Research, University of Minnesota, Minneapolis, Minnesota. [6]Koch Institute for Integrative Cancer Research, Massachusetts Institute of Technology, Cambridge, Massachusetts. [7]Center for Integrated Diagnostics, Department of Pathology, Massachusetts General Hospital, Harvard Medical School, Boston, Massachusetts. [8]Stephen E. and Catherine Pappas Center for Neuro-Oncology, Division of Hematology/Oncology, Department of Neurology, Massachusetts General Hospital, Harvard Medical School, Boston, Massachusetts. [9]Dana-Farber/Harvard Cancer Center, Boston, Massachusetts.

**Note:** Supplementary data for this article are available at Clinical Cancer Research Online (http://clincancerres.aacrjournals.org/).

**Corresponding Authors:** Ovidiu C. Andronesi, Massachusetts General Hospital, Harvard Medical School, Building 149, Thirteenth Street, Charlestown, MA 02129. Phone: 617-643-6864; Fax: 617-726-7422;. E-mail: ovidiu@nmr.mgh.harvard.edu; and Daniel P. Cahill, E-mail: cahill@mgh.harvard.edu

**doi:** 10.1158/1078-0432.CCR-15-0656

## Translational Relevance

IDH mutations are at the center of genetic, epigenetic, and molecular alterations that define a distinct subtype of glioma patients. As a direct product of mutant IDH enzyme, 2HG can probe enzymatic activity and target modulation by inhibitory drugs. Hence, measurements of 2HG levels can accelerate clinical trials and translation of IDH mutant–specific glioma therapies. However, repeated invasive sampling of tumor tissue is generally not feasible in glioma patients and noninvasive measurements of 2HG are necessary. *In vivo* imaging of 2HG levels using magnetic resonance spectroscopy (MRS) provides a safe and effective way to probe mutant IDH glioma patients. Our three-dimensional MR spectroscopic imaging of 2HG has the temporal stability and spatial coverage required to monitor treatment response and tumor heterogeneity in IDH-mutant glioma patients, and can be easily incorporated into clinical trials of targeted therapies as a precision medicine tool to determine objective response rates.

Hence, 2HG may serve as a unique biomarker to probe IDH-mutant tumor burden, cancer mechanisms, and therapeutic opportunity. This possibility is based on a powerful combination of mutually exclusive events: (i) IDH mutation is an early oncogenic event in gliomas (12), (ii) it is not found outside the tumor volume in patients harboring this mutation (13), (iii) IDH-mutant cancer cells produce very high levels of 2HG (8), and (iv) only trace levels of 2HG are found in IDH wild-type cells where it is cleared rapidly by 2HG dehydrogenases (8).

The markedly increased intracellular concentration of 2HG, up to 5 to 35 mmol/L (8), exceeds the sensitivity threshold for *in vivo* magnetic resonance spectroscopy (MRS). Early work by our group (14) and others (15, 16) has reported on the feasibility of single-voxel or single-slice MRS detection of 2HG in IDH-mutant glioma patients. Unambiguous *in vivo* detection of 2HG by conventional MRS is challenging, and special editing spectroscopic methods were designed (14, 15) to disentangle the 2HG signal from overlapping signals from metabolites with similar structure.

While initial studies (14–18) focused on 2HG imaging for diagnosing IDH-mutant gliomas, currently the interest has shifted towards longitudinal 2HG imaging for monitoring treatment response in IDH-mutant patients. Nevertheless, the existing data suggest that in addition to its diagnostic/prognostic value (7, 19), 2HG may be also predictive of treatment outcome (20). It is expected that reliable longitudinal quantitative measurement of 2HG levels in response to treatment would accelerate clinical trials, either as a pharmacodynamic marker for small-molecule inhibitors (20) that block the production of 2HG by mutant IDH, or as an efficacy marker for drugs that selectively kill IDH-mutant tumors based on synthetic lethality (21, 22). This is highly relevant for intracranial gliomas where multiple patient biopsies to test activity of novel therapeutics in a longitudinal study are often not feasible. On the other hand, it has been shown in previous studies that MRS can be safely performed to monitor treatment response in glioma patients (23, 24).

Because of tumor heterogeneity and the physical remodeling of tumor–brain structure during treatment course, regional changes of 2HG levels need to be measured longitudinally over the entire tumor volume. The imaging requirements for monitoring tumor treatment response are more stringent than for diagnosis, and this has not been demonstrated yet for 2HG. In comparison, for diagnosing IDH mutation the one time presence or absence of 2HG signal is sufficient (14, 15), while for tracking response accurate changes in 2HG levels have to be reliably measured in the same anatomical location over time.

In the current work, we hypothesized that a decrease in 2HG levels would be measureable by *in vivo* MRS in mutant IDH glioma patients as a result of antitumor therapy. As only the mutant IDH glioma cells produce 2HG, a reduction in the number of tumor cells or impairment of their metabolism would result in decreased 2HG levels. To test our hypothesis, we used a recently developed three-dimensional (3D) MRS imaging (MRSI) sequence (25) that can selectively edit metabolites of interest, such as 2HG, with increased temporal stability and spatial coverage. Existing data suggest that IDH-mutant gliomas are more radiosensitive compared with their wild-type counterparts (26, 27), hence a 2HG reduction may be observed in patients treated with radiotherapy. Therefore, we tested our hypothesis in a prospective longitudinal study of a cohort of IDH-mutant gliomas patients undergoing radiation, and evaluated the potential of noninvasive 3D 2HG quantification for response assessment.

For this study, we further propose a novel analytic framework, which we label functional spectroscopic map (fSM), as a metric to quantify spatiotemporal changes of metabolite levels. Importantly, 3D fSM provides comprehensive tumor metabolic information that cannot be captured by a single mean value of metabolite levels. In this respect, fSM of 2HG is similar to functional diffusion map (fDM; ref. 28) based on apparent diffusion coefficient (ADC) that showed increased value over mean ADC values for treatment monitoring of glioblastoma patients (29). It is expected that tumor regions with decreased 2HG/Cre and/or increased ADC would correlate with treatment response. Results from 3D 2HG fSM were compared against other imaging modalities for determining treatment response such as RANO criteria (4, 5) and diffusion MRI (29).

In our study, we found a statistically significant decrease of mean 2HG levels and tumor volume with quantifiable 2HG between pre- and posttreatment scans, early after completion of radiotherapy. In addition, correlation between changes of 2HG levels and clinical improvement supports the hypothesis that 2HG could be used as an endpoint to determine objective response rates complementary to traditional clinical outcome criteria in IDH-mutant patients.

## Materials and Methods

### Patient population

Glioma patients (WHO grades II–IV) seeking clinical care at the Pappas Center of Neuro-Oncology from Massachusetts General Hospital (Boston, MA) were selected for our study over the last year. Inclusion criteria specified: (i) independent confirmation of mutant IDH and (ii) clinical indication for radiation and/or chemotherapy. Standard external beam radiotherapy (photons) was administered focal in 2 Gy/day fractions for 5 days over a 6-week period. Focal radiotherapy included a 2 to 3 cm margin beyond tumor or resection margin. Chemotherapy was administered using the oral methylating drug temozolomide, at a dose 75 mg/m$^2$/day, 7 days per week for the same duration as radiotherapy. Temozolomide was also continued after the completion

of radiation (150–200 mg/m$^2$/day, days 1–5 of a 28-day cycle, six cycles). All patients had surgical procedures (i.e., diagnostic biopsy, subtotal, or gross-total resection) but none received prior adjuvant treatment. Exclusion criteria were patients who could not be safely imaged with MRI. A number of 25 patients ($N = 25$) were consented with an approved IRB protocol and enrolled in the imaging study. Patients are listed in Supplementary Tables S1 and S2.

### Image acquisition

All images were acquired on a clinical 3T MR scanner (Tim Trio, Siemens) with a 32-channel head coil. A robust 3D MRSI sequence for 2HG imaging was newly developed (25) by integrating three highly optimized modules: (i) adiabatic J-difference spectral editing MEGA-LASER, (ii) spiral spectroscopic imaging, and (iii) real-time prospective motion correction, shim update with reacquisition. This sequence efficiently edits 2HG signal while minimizing subtraction errors caused by subject motion or scanner instability. Details of the pulse sequence are provided in Supplementary Fig. S1.

The acquisition parameters of the 3D MRSI sequence were: TR = 1,600 ms, TE = 68 ms, FOV = 200 × 200 × 200 mm$^3$, VOI = 100 × 80 × 50 mm$^3$, 20 mm isotropic voxels, acquisition matrix 10 × 10 × 10 zero-filled to 16 × 16 × 16, NA = 20, acquisition time 9 minutes and 55 seconds. Our choice of spatial resolution favored the SNR, but higher resolutions are technically possible for the same acquisition time. The timing of the MEGA-LASER excitation was optimized by simulations and phantom measurements for the maximum 2HG signal. MEGA pulses were applied in an interleaved fashion at 1.9 ppm (ON) and 7.5 ppm (OFF) to edit the 2HG signal (H$\alpha$) at 4.02 ppm. To assess repeatability, 3D MRSI was acquired twice at the baseline in 6 patients. For test–retest, patients were taken out from the scanner and repositioned between first and second 3D MRSI.

In addition, 3D T2 weighted (TR/TE = 3200/420 ms, FOV = 256 × 256 × 176 mm$^3$, matrix = 256 × 256 × 176) and two-dimensional fluid-attenuated inversion recovery (FLAIR, TR/TI/TE = 10,000/2,500/70 ms, FOV = 220 × 186 × 138 mm$^3$, matrix = 256 × 192 × 23) images were acquired. In 20 patients, diffusion tensor imaging (DTI) was also acquired (TR/TE = 7,980/84 ms, b-values = 0/700 s/mm$^2$, gradient directions = 12, FOV = 236 × 236 × 118 mm$^3$, matrix = 128 × 128 × 64).

To reproduce positioning across visits for each patient, the online automatic slice positioning (AAscout, ref. 30) was used during acquisition of all imaging data.

### Image processing

The difference (ON−OFF) and OFF spectra from each voxel of the VOI (∼200 voxels per VOI) were fitted with LCModel (31) software using the corresponding simulated basis sets for the MEGA-LASER sequence. Difference spectra were used to quantify 2HG and Glx (glutamate and glutamine). OFF spectra were used to quantify total choline (tCho), creatine (Cre), lactate (Lac), and N-acetyl-aspartate (NAA). Cramer–Rao lower bound (CRLB) less than 25% (relative CRLB) as calculated by LCModel was considered acceptable for goodness of fits (see the note and references at the end of Supplementary Data for rationale of CRLB threshold). 3D metabolic maps were further constructed using a combination of MINC (Montreal Neurological Institute), FSL (FMRIB Software Library), and MATLAB (Mathworks) software tools. Relative metabolic maps were obtained for 2HG, Glx, Lac, tCho, and NAA as ratio to Cre. Ratios to Cre were preferred to water because of edema, cysts, and surgical cavities that need to be accurately segmented, while Cre excludes these confoundings. All metabolic maps were coregistered to anatomical T2w, FLAIR, and ADC images for each visit.

Coregistration of T2w, FLAIR, and ADC images obtained at different time points was performed using the robust register method of Freesurfer (32) to a common middle space. The same transformations were applied to coregister the corresponding 3D metabolic maps. In addition, AAscout ensured prospectively that images and spectral maps were identically positioned at each visit.

Difference maps were calculated by voxel-wise subtraction between coregistered post- and pretreatment scans for metabolic and ADC maps. Functional spectroscopic (fSM) and diffusion (fDM) maps were obtained by thresholding the 2HG/Cre and ADC difference maps, respectively. Functional mapping classifies voxels in three categories: (i) decrease, (ii) stable, and (iii) increase according to a statistically significant functional threshold. The functional threshold for difference 2HG/Cre (Δ2HG/Cre) was taken as the 95% confidence interval (95% CI) of the test–retest distribution. The normality of test–retest Δ2HG/Cre distribution was verified by Kolmogorov–Smirnov test. The 95% CI of test–retest Δ2HG/Cre distribution was found to be 0.11, hence voxels with $\Delta 2HG/Cre < -0.11$ were considered to have decreased 2HG/Cre, voxels with $\Delta 2HG/Cre \in (-0.11–0.11)$ were considered stable, and voxels with $\Delta 2HG/Cre > 0.11$ were considered to have increased 2HG/Cre. For difference ADC (ΔADC), a functional threshold of 0.4 μm$^2$/ms representing the 95% CI of gray and white matter distribution was used, as proposed by Ellingson and colleagues (33).

Tumor regions of interest (ROI) were manually outlined on the FLAIR images to include tumor tissue and infiltrating peritumoral edema, with exclusion of surgical cavities, cysts, or necrosis areas. For each ROI multiple imaging biomarkers were calculated: (i) FLAIR tumor volumes, (ii) mean, median, and 95% CI for 2HG/Cre, Glx/Cre, Lac/Cre, tCho/Cre, NAA/Cre, (ii) mean, median, and 95% CI for ADC, (iv) volume of voxels with quantifiable 2HG/Cre > 0.1, and (v) volume of voxels with decreased, increased, and stable 2HG/Cre and ADC, respectively.

### Statistical analysis

Differences in imaging biomarkers between post- and pretreatment scans were deemed significant at a level of $P < 0.05$ using two-sided Student $t$ test. Correlations between 2HG and other imaging biomarkers were calculated using Pearson product-moment correlation coefficient. Multivariate linear regression (general linear model) was performed using KPS as dependent variable and 2HG/Cre, age, and grade as covariates. All statistical analysis was performed with the statistical package of MATLAB.

### Genomic analysis

IDH mutational status was confirmed by IHC analysis using an anti-human R132H antibody (DIANOVA; ref. 34), or by genetic sequencing (SNaPshot; ref. 35). In addition, molecular markers such 1p/19q codeletion (36) and MGMT promoter methylation (37) were tested using FISH and PCR, respectively (35).

### Clinical and radiologic evaluation

Patients were evaluated clinically and radiologically by the treating neuro-oncologist and radiographic images were centrally reviewed by (to A.S. Chi and D.P. Cahill). Karnofsky performance status (KPS; ref. 38) was used to assess functional improvement or

decline. Primary clinical endpoints such as overall survival (OS) and progression-free survival (PFS) were limited due to length of follow-up time. Response Assessment in Neuro-Oncology (RANO; refs. 4, 5) criteria were used to determine whether patients had complete response (CR), partial response (PR), minor response (MR), stable disease (SD), or progressive disease (PD).

## Results

### Optimization of 3D MRSI editing of 2HG

The MEGA-LASER editing was optimized before the start of the longitudinal study. Detailed results pertaining to this phase are shown in the Supplementary Data (Supplementary Figs. S2–S4). In Supplementary Fig. S2, the efficiency of 2HG editing of MEGA-LASER (25) is compared with MEGA-PRESS and PRESS-97 (PRESS, TE = 97 ms), the other two sequences which were previously demonstrated (15) for 2HG detection in patients. MEGA-LASER was found to provide 60% signal increase compared with MEGA-PRESS, and 90% of the signal of PRESS-97. When considering the range of B1 field inhomogeneity at 3T, the MEGA-LASER has improved performance, yielding 94% and 115% of the PRESS-97 signal for a variation of −15% to +15% B1 amplitude, respectively (Supplementary Fig. S3). Real-time correction (25) of subtraction errors due to patient motion or scanner instability is shown in Supplementary Fig. S4.

### Longitudinal imaging

Twenty-five patients ($N = 25$) were enrolled and imaged in this study. Thirteen ($N = 13$) patients were imaged twice: (i) a pretreatment baseline scan 1 to 14 days before starting adjuvant treatment, and (ii) a posttreatment follow-up scan acquired in the time interval of 1 to 3 months after the end of radiochemotherapy. The remaining 12 patients had only baseline scans either due to change of the treatment plan or lack of compliance. Out of the 13 patients imaged longitudinally, 4 had extensive surgical resection and 2HG levels could not be detected on the postoperative scan. The baseline metabolite levels from all 25 patients are given in Supplementary Table S1. The 9 patients that had only biopsy or subtotal resection with 2HG present at baseline and follow-up are listed in Supplementary Table S2 with their demographic, genomic, molecular, histologic, radiologic, and clinical data. Note that any surgical procedure was done before the baseline scan, and no tumor was removed between baseline and follow-up scans.

Representative metabolic maps obtained from the pre- and posttreatment scans are shown in Fig. 1. Comparing the intra-scan

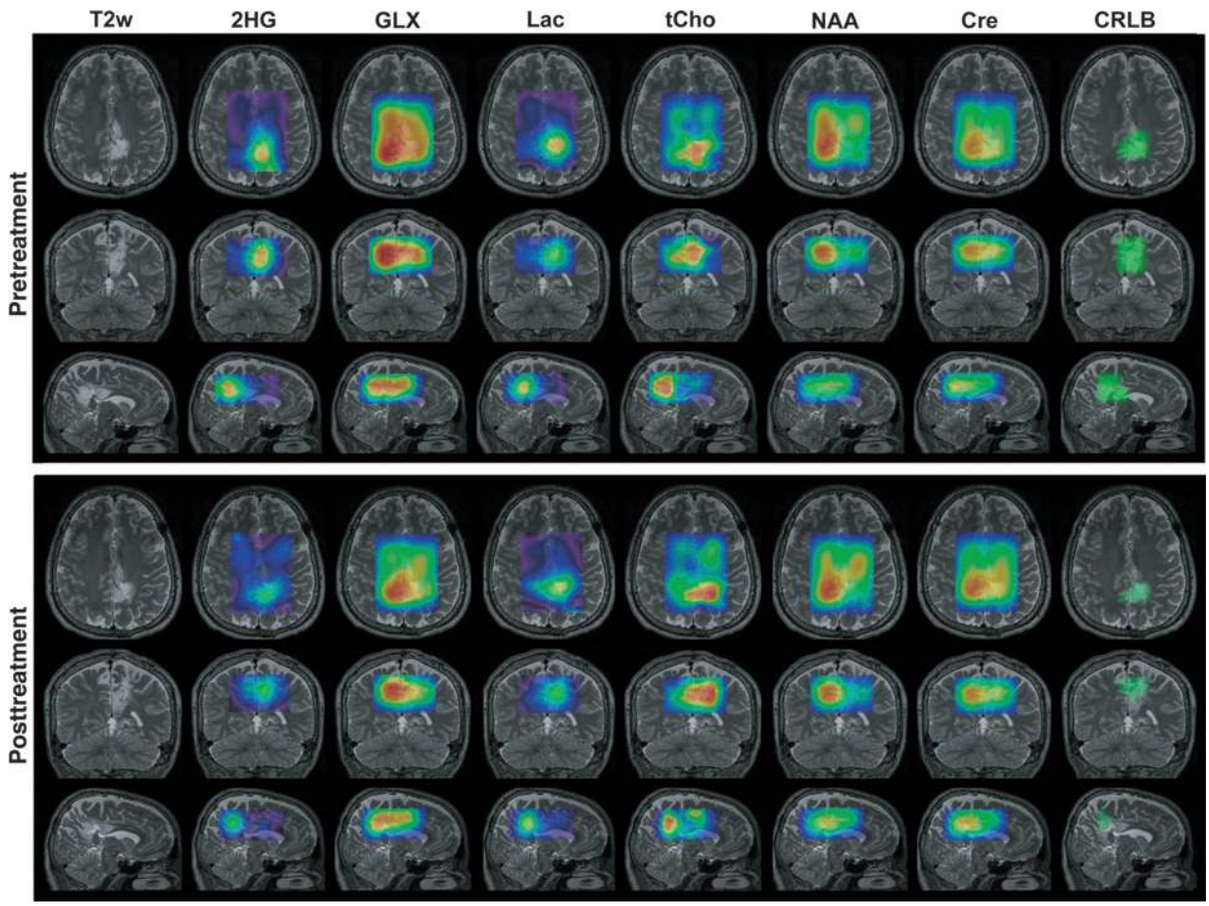


**Figure 1.**
3D metabolic maps in a mutant IDH glioma patient (grade II, astrocytoma, R132C) before and after radiotherapy. The pre- and post-treatment maps of each metabolite are scaled to the same intensity scale. In the last column, the mask of CRLB < 25% is shown for 2HG goodness of fit by LCModel.

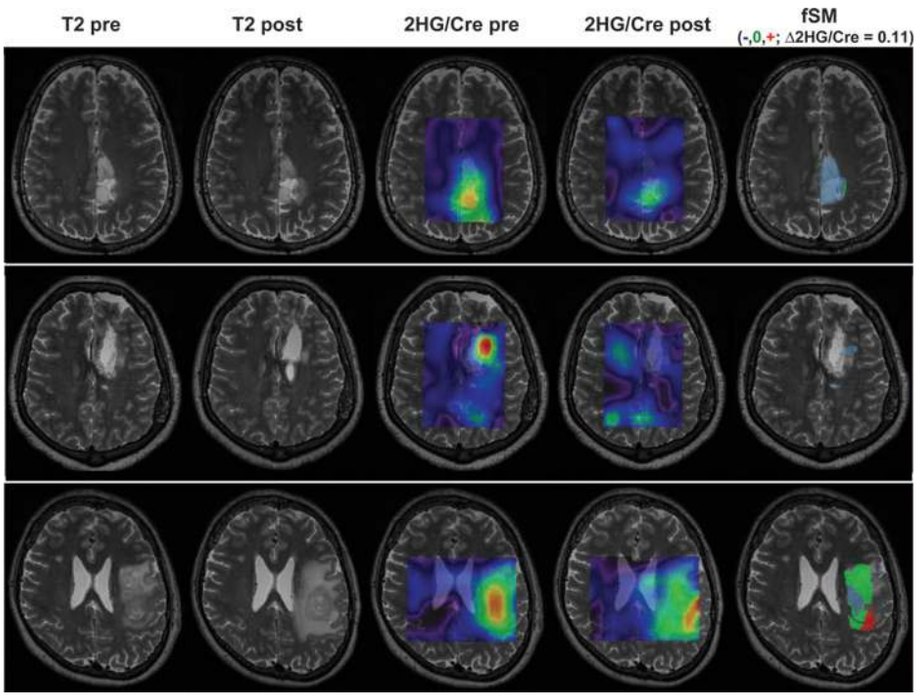


**Figure 2.**
Functional spectroscopic maps (fSM) of 2HG/Cre. fSM from 3 patients are shown: upper patient grade II (WHO) astrocytoma, middle patient grade III (WHO) anaplastic astrocytoma, and lower patient grade IV (WHO) glioblastoma. A threshold $\Delta$2HG/Cre = 0.11 was used to classify voxels as decreased (blue), increased (red), or stable (green) 2HG/Cre. The fSM maps are masked by the CRLB < 25% mask.

maps (either pre- or posttreatment), regions of high 2HG correspond to regions of high lactate and choline, and to regions of reduced Glx (glutamate and glutamine) and NAA, respectively. Comparing the inter-scan maps (pre- vs. posttreatment), it can also be seen that 2HG has the largest change among all metabolites with treatment. The metabolic maps corresponding to the acquired 3D MRSI matrix are shown before image interpolation in Supplementary Fig. S5.

Difference and OFF spectra from voxels selected in the tumor and contralateral normal appearing white matter before and after treatment, respectively, are shown in Supplementary Fig. S6. The edited 2HG signal at 4.02 ppm can be clearly distinguished only in the difference spectra in the tumor, with reduced amplitude after treatment. In addition, other metabolites can be identified in the OFF spectra (NAA, choline, creatine, and lactate), or are coedited in the difference spectra (GABA+ and Glx).

In Fig. 2, three examples of functional spectroscopic maps (fSM) for 2HG/Cre are shown from a WHO grade II, WHO grade III, and WHO grade IV patient, respectively. Lower grade (WHO-II, WHO-III) and smaller tumors seem to have a more uniform response (decrease) of 2HG/Cre to treatment. Higher grades (WHO-IV) typically present with a larger tumor volume and show a more heterogeneous treatment response with regions of decreased, stable, and increased 2HG/Cre within the tumor after treatment. The distribution of $\Delta$2HG/Cre values for test–retest and longitudinal scans is shown in Supplementary Fig. S7. For test–retest, the $\Delta$2HG/Cre values follow a single normal distribution with a mean of $-0.022$ and 95% CI of $\pm 0.115$. For the longitudinal scans, the $\Delta$2HG/Cre values may be arranged on two normal distributions with a mean/95% CI of $-0.45/\pm 0.19$ (voxels of large response), and a mean/95% CI of $-0.13/\pm 0.15$ (voxels of low response). The two distributions showed that there were approximately three times less voxels of large response compared with voxels of low response. Comparison of fSM and functional diffusion maps (fDM) maps is shown in Supplementary Fig. S8. It was noticed that regions of decreased 2HG/Cre partially overlap with regions of increased apparent diffusion coefficient (ADC), suggestive of reduction in cellular density associated with treatment response.

### Quantification of biomarkers

In Fig. 3, histograms of 2HG/Cre values within tumor ROI are shown for all patients for both pre- and posttreatment scans. In general, a shift toward lower and a narrower range of 2HG/Cre values are seen in posttreatment scans as compared with pretreatment scans. Bar plots are shown in the enclosed bottom panel for pre- and post-median values of 2HG/Cre (Fig. 3A), pre- and post-fractional volumes of 2HG/Cre (Fig. 3B), and fractional volumes of 2HG/Cre changes from fSM (Fig. 3C). Typically, larger differences between pre- and post-treatment values were noticed for lower grade patients. In particular, the effect of tumor heterogeneity on changes of 2HG levels can be noticed in Fig. 3C, showing tumor volumes where 2HG levels were decreased, stable, and increased, respectively. Fractional changes for all 2HG/Cre parameters are listed in Table 1. Fractional changes for all imaging biomarkers are provided in Supplementary Table S3.

Group mean values and 95% CI of all imaging biomarkers over tumor ROIs are listed in Table 2. The only biomarkers that demonstrated a statistically significant change between pre- and post-treatment scans were 2HG/Cre ($P = 0.0069$) and the volume of 2HG/Cre ($P = 0.0406$). Across the patient group, the mean pretreatment 2HG/Cre was 0.36 (95% CI = $\pm 0.09$) and the mean posttreatment 2HG/Cre was 0.2 (95% CI = $\pm 0.05$). The mean pretreatment volume of 2HG/Cre was 7.65 $cm^3$ (95% CI = $\pm 6.55$ $cm^3$), whereas the mean posttreatment volume of 2HG/Cre was 4.5 $cm^3$ (95% CI = $\pm 4.43$ $cm^3$).

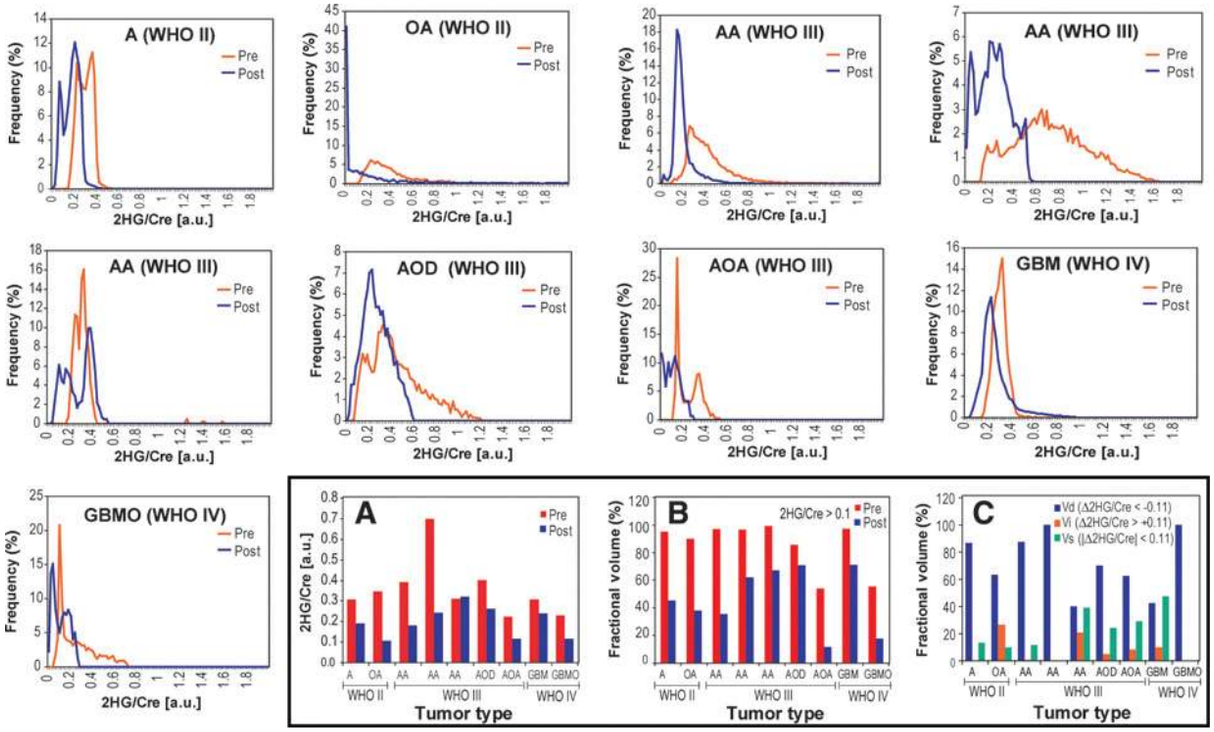


**Figure 3.**
Histograms for 2HG/Cre values within tumor ROI for all patients: posttreatment histograms (blue line) compared with pretreatment histograms (red line). Bottom panel includes bar plots for: median 2HG/Cre (A), fractional tumor volume of 2HG/Cre (>0.1; B), and fractional volumes of decreased, stable and increased 2HG/Cre (Δ2HG/Cre = 0.11; C). Fractional volumes are calculated as the ratio of 2HG/Cre or Δ2HG/Cre volume within specified thresholds over the total volume of tumor outlined on FLAIR images and masked by CRLB < 25%. Abbreviations: A, Astrocytoma; AA/OA, Anaplastic/Oligo-astrocytoma; AOD/A, Anaplastic-oligodendroglioma/astrocytoma; GBM(O), Glioblastoma (with oligodendroglial component).

Box plots of tumor mean fractional changes of metabolites are shown in Fig. 4A. The median fractional change of 2HG/Cre −41.87% (95% CI = ±14.62%, median = 48.17%), while the median fractional change of 2HG/Cre volume was −39.07% (95% CI = ±9.3%). The box plots of fractional volumes of decreased, increased, and stable 2HG/Cre and ADC are plotted in Fig. 4B. A reduction in the number of tumor cells due to treatment is expected to correlate with the fractional volume of decreased 2HG/Cre and the fractional volume of increased ADC. We found that the mean fractional volume of decreased 2HG/Cre was 58.2% (95% CI = ±15.8%) and the mean fractional volume of increased ADC was 18.2% (95% CI = ±13.6%). The relationship between the quality of 2HG data and the apparent (FLAIR) tumor size is presented in Supplementary Fig. S9, showing a trend for higher SNR and lower CRLB of 2HG in tumors that have larger FLAIR volumes, albeit not statistically significant. Note that within the mask of 2HG goodness of fit (e.g., Fig. 1, last column), a significant number of voxels had relative CRLB lower than 20%, as indicated in Supplementary Fig. S9.

### Correlation of clinical and imaging data

Univariate linear regression was first used to establish whether serial changes of 2HG correlated with serial changes in the KPS scores. We separately tested all metrics calculated for 2HG/Cre (mean difference, volume, and fractional decreased volume), and we found that the fractional volume of decreased 2HG/Cre correlated strongest with the increase of KPS ($R^2 = 0.88$, $P = 0.002$). The scatter plot of KPS change versus the fractional volume of decreased 2HG/Cre is shown in Fig. 4C. Interestingly, the patient with RANO progressive disease has also the lowest

**Table 1.** Fractional values for several 2HG metrics: median 2HG/Cre, volume of 2HG/Cre>0.1, volume of decreased 2HG/Cre (fVd), volume of increased 2HG/Cre (fVi), and volume of stable 2HG/Cre (fVs)

| Patient # | 2HG/Cre | Volume (2HG/Cre>0.1) | fVd (Δ<−0.11) | fVi (Δ>0.11) | fVs [Δ∈(−0.11, +0.11)] |
|---|---|---|---|---|---|
| 1 | −37.37 | −50.09 | 60.01 | 0.00 | 39.99 |
| 2 | −69.32 | −51.87 | 58.23 | 24.58 | 17.18 |
| 3 | −54.01 | −61.55 | 76.74 | 0.86 | 22.41 |
| 4 | −65.39 | −34.61 | 99.12 | 0.00 | 0.88 |
| 5 | 2.88 | −32.15 | 24.82 | 8.75 | 66.43 |
| 6 | −34.34 | −14.86 | 60.76 | 1.09 | 38.15 |
| 7 | −48.09 | −42.53 | 49.11 | 3.29 | 47.59 |
| 8 | −22.30 | −26.29 | 19.78 | 7.95 | 72.27 |
| 9 | −48.89 | −37.70 | 58.01 | 0.00 | 41.99 |

NOTE: All values are given as percentage change (%). Fractional changes of all imaging biomarkers are given in Supplementary Table S3.

**Table 2.** Mean and 95% CI of imaging biomarkers across patient group

| Imaging biomarker | Pre | Post | Difference | *P* |
|---|---|---|---|---|
| 2HG/Cre | 0.36 ± 0.09 | 0.20 ± 0.05 | −0.16 ± 0.09 | 0.0069 |
| GLX/Cre | 1.06 ± 0.18 | 0.99 ± 0.18 | −0.07 ± 0.10 | 0.2278 |
| Lac/Cre | 0.35 ± 0.16 | 0.30 ± 0.12 | −0.05 ± 0.04 | 0.0576 |
| tCho/Cre | 0.33 ± 0.09 | 0.30 ± 0.09 | −0.03 ± 0.04 | 0.1455 |
| NAA/Cre | 0.83 ± 0.10 | 0.80 ± 0.11 | −0.02 ± 0.06 | 0.4686 |
| tCho/NAA | 0.47 ± 0.19 | 0.41 ± 0.15 | −0.06 ± 0.11 | 0.2543 |
| ADC ($\mu m^2$/ms) | 1.29 ± 0.09 | 1.32 ± 0.11 | 0.03 ± 0.04 | 0.2075 |
| Volume 2HG/Cre ($cm^3$) | 7.65 ± 6.55 | 4.50 ± 4.43 | −3.15 ± 2.53 | 0.0406 |
| Volume FLAIR ($cm^3$) | 35.90 ± 17.36 | 38.59 ± 20.57 | 2.69 ± 7.61 | 0.5075 |

NOTE: The median over the tumor ROI was considered for the biomarkers of each patient. Values are given for pre-, post-treatment, and the difference (post−pre) treatment.

fractional volume of decreased 2HG/Cre and the largest decline of KPS, whereas one of the patients with minor response had the largest fractional volume of decreased 2HG/Cre and largets improvement of KPS. The change in FLAIR volume and mean ADC did not correlate with KPS scores. Results from a general linear regression model including tumor grade and age besides the fractional volume of decreased 2HG/Cre are given in Supplementary Table S4, with the caveat that the number of patients was not enough for the number of independent variables.

## Discussion

*In vivo* MRS has the unique ability to probe specifically and noninvasively IDH-mutant gliomas by measuring the IDH mutant–specific oncometabolite 2HG. Compared with single-voxel or single-slice methods (14, 15), the 3D MRSI imaging technique reported here provides complete spatial coverage of tumors and exploits the full potential of advanced image analysis. 3D mapping of 2HG and other metabolites have the advantage of accounting for tumor heterogeneity and may be especially important for longitudinal studies, because the change in size, shape, and molecular composition of tumors during treatment makes positioning of a single voxel or a single slice difficult to match precisely over time. Indeed, 3D imaging has been shown to reduce variance in longitudinal MRS studies (39), likely because it is not affected by the sampling bias of single-voxel methods, or for that matter, of invasive biopsies. In addition to obtaining a single mean or median 2HG/Cre value for a tumor, several more useful metrics can be computed from 3D MRSI data, such as histogram and volumetric analysis. Similar to functional diffusion maps (28, 29), which showed increased clinical utility over mean ADC value in longitudinal studies of glioma patients, fSM can be constructed to obviate regional significant changes of 2HG. While we noticed a trend between the decrease of 2HG and the increase of ADC in response to therapy, we did not find a statistical significant correlation between these two imaging biomarkers. This limitation of our study may require further investigation to demonstrate whether 2HG is a biomarker that presents with an earlier treatment response as compared with ADC.

The observed 2HG levels are linked to NADPH (40) depletion and the impaired reductive capacity of IDH-mutant cells. Therefore, 2HG quantification could probe directly the potential mechanisms of radiation damage (26, 27) in IDH-mutant cells and decrease of tumor burden. In our study, the fractional volume of decreased 2HG/Cre derived from 3D fSM has been found to correlate stronger than the median 2HG/Cre with KPS, used as a standard measure of clinical status. Although KPS is often a secondary endpoint in clinical studies and not a primary endpoint such as the gold-standard endpoints of OS or PFS, KPS is a well-established prognostic factor in gliomas and has been used in conjunction with imaging to predict survival (41). Although clinical scoring systems such as KPS are known to be subjective with large interobserver variability, clinical assessments are an integral part of the criteria used to establish imaging endpoints

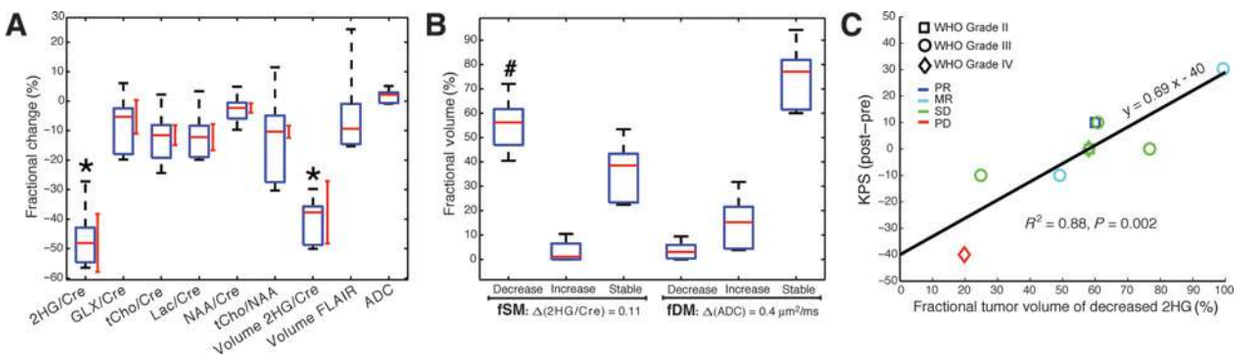


**Figure 4.**
Box plots of imaging biomarkers and clinical correlation. A, fractional changes [(post−pre)/pre ×100,%) of metabolite ratios, ADC mean tumor ROI values, and tumor volumes of 2HG/Cre (>0.1) and FLAIR. Vertical red lines indicate the variability of test–retest measurements. Stars indicate statistical significant change ($P < 0.05$) between pre- and posttreatment scans. B, fractional volumes of decreased, increased, and stable 2HG/Cre and ADC, respectively. #, statistical significant correlation with KPS clinical outcome. C, univariate linear regression of KPS (post−pre change) and the fractional tumor volume of decreased 2HG/Cre (PR, partial response; MR, minor response; SD, stable disease; PD, progressive disease by RANO criteria).

(4, 5). Ultimately, 2HG imaging correlation with OS and PFS in this subset of patients will be informative; however, these endpoints will require many more years of follow-up, as retrospective studies (7, 42) indicate these patients have a median PFS of >50 months and median OS of >100 months.

Multiple metabolites can be quantified from the same 3D MRSI dataset allowing further exploratory studies of aberrant metabolic networks and pathways in tumors. In our data, the tumor ROI median value of 2HG/Cre was found positively correlated with that of Lac/Cre in pretreatment scans ($R^2 = 0.84$, $P = 0.0047$), but correlation was not statistically significant in posttreatment scans ($R^2 = 0.13$, $P = 0.744$). It is possible that the increased lactate levels in IDH-mutant gliomas may be the result of Warburg effect due to silencing of lactate dehydrogenase A (43). In addition, monocarboxylate transporters (MCT) are responsible for lactate transport, and modulation of MCT has been suggested as potential therapeutic in glioma (44).

Conversely, the tumor ROI median value of 2HG/Cre was negatively correlated with that of Glx/Cre in posttreatment scans ($R^2 = -0.86$, $P = 0.0026$), but correlation was not statistically significant in pretreatment scans ($R^2 = -0.36$, $P = 0.34$). Negative correlation between 2HG and glutamate/glutamine levels may be possible in mutant IDH through a shunting effect. Glutamine via glutamate is used to produce α-ketoglutarate that is further a substrate for 2HG synthesis. Glutamine represents the major source of 2HG production (8) in mutant IDH cells and is also a major source for tricarboxylic acid cycle (TCA) anaplerosis, suggesting glutaminolysis (21) as a plausible therapeutic intervention. Lower glutamate and glutamine levels have been measured in mutant versus wild-type IDH cell cultures (45), while results from animal models have yielded a more complex fate of glutamate and glutamine (46, 47). To our knowledge, our findings are the first corroborating *in vivo* evidence in patients suggesting that changes in glutamate and glutamine may accompany the loss of 2HG production with glioma treatment.

Except of 2HG no other metabolite showed a statistical significant effect in the posttreatment scan. In particular, choline that is the most measured metabolite for monitoring cancer progression and response by MRS was not sensitive to treatment changes within 1 to 3 months posttreatment, highlighting the potential of 2HG as an earlier imaging marker sensitive to treatment effects. In an earlier study (23) of temozolomide in glioma patients, choline MRS at 3 months was not significantly different from baseline, while a more recent study (24) has shown that Cho/Cre at 3 months predicts tumor response. The difference between our results and of previous studies may be explained by both different patient population (all IDH mutant) and treatment (radiotherapy). Arguably, choline is not a specific marker for tumor cells, and the levels of choline can change also due to inflammation, gliosis, and other biologic responses of nontumor cells, while 2HG accumulates only in the mutant cells.

Special attention and careful analysis need to be exercised when computing functional maps. The difference method that is at the core of the functional mapping requires accurate longitudinal coregistration of baseline and follow-up images, especially of the tumor ROI, which is not a trivial problem. Except for rigid misalignment of head position which is easier to correct, more challenging situations can arise from deformation within the brain due to the tumor growth or treatment. To minimize rigid displacement, we have used automatic alignment of baseline and follow-up MRSI during the acquisition coupled with real-time motion correction, and followed by post-processing head coregistration. On the other hand, because IDH tumors grow very slow and the time between two scans is short the internal brain deformation is minimal, and its effect at the spatial resolution of MRSI may be minimal too.

In addition, the quality of MRSI is critical for the end results. While our methodology has improved robustness designed to increase the number of patients from which good quality MRSI can be obtained, there will be a limited number of cases, in particular, with tumor location in areas of large B0 inhomogeneity close to air cavities (sinuses, nasal) which will be challenging for MRSI. For these situations further development is necessary.

Several limitations exist in our study. There are few patients of different glioma grades and histologic subtypes, limiting our ability to assess correlation between 2HG imaging and histologic subgroups. The utility of 2HG imaging to predict OS and PFS cannot yet be investigated, as this determination will require at least 5 to 10 years of follow-up after baseline imaging, due to the prolonged clinical course of mutant IDH gliomas. The value of 2HG imaging for stratifying patients according to their RANO (4, 5) criteria treatment response (CR, PR, MR, SD, PD) could only be partially compared, as RANO criteria are based upon mixed glioma cohorts (IDH wild-type and mutant) and differ across WHO histologic grades [high-grade, WHO grades III and IV (4), versus low-grade, WHO grade II (5)]. We did nevertheless observe a correlation of 2HG imaging with high-grade RANO criteria for patients that show progressive disease, but other patient categories are underrepresented at this interface between the two paradigms of glioma classification (histologic vs. molecular). Our methods will only apply to the molecularly homogeneous population of IDH-mutant gliomas, a cohort for which objective clinical response criteria are not yet established. Existing data suggest that mutant IDH glioma of different WHO grades may be more similar, than for example wild-type and mutant glioma of the same WHO grade (48). In addition, it is known that the peak "best response" of traditional radiographic response criteria are often delayed (49) with respect to metabolic activity, and IDH-mutant tumors have typically less contrast enhancement (48, 50) compared with wild-type IDH gliomas.

A 2HG/Cre threshold of 0.115 was found to be statistically significant for change of 2HG levels. Assuming a total Cre level between 8 and 10 mmol/L (Supplementary Fig. S7 and Supplementary Ref. S7), the 2HG/Cre threshold of 0.115 would correspond to a 2HG level around 1 mmol/L, which corresponds to the minimum concentration that can be detected by *in vivo* MRS. Interestingly, the 0.115 threshold compared with the range (0.15–0.45) of 2HG/Cre values is similar to what was observed for ADC [threshold of $0.4 \times 10^{-3}$ mm$^2$/s for a range of $(0.5–1.5) \times 10^{-3}$ mm$^2$/s, (33)]. However, a longer study and more subjects will be required to establish the optimal imaging time point and the threshold of 2HG as an endpoint that can be used to determine or predict the objective response rate in this patient population.

Nevertheless, we demonstrate that longitudinal 3D functional imaging of 2HG is clinically feasible for noninvasive treatment monitoring. Our methodology combines imaging and genomics, and 2HG imaging is a clear example for the value of imaging genomics (radiogenomics) paradigm (50) in IDH-mutant gliomas. As an imaging technique, 3D fSM has the benefit of posing minimal risks to patients with the possibility to repeat examinations as many times as necessary. Compared with other molecular

imaging modalities (PET, SPECT) the 3D MRSI is cost effective, easy to perform, and not confounded by the permeability of blood–brain barrier. Our novel method represents a major advance over prior point-diagnostic methods (14–16), and has immediate practical implications for patients with mutant IDH gliomas, who can now enter fSM surveillance after initial treatment. In contrast with other MRI modalities that can be used to assess treatment response (27, 50), our methods provide quantitative and mechanistic information about IDH enzymatic activity, metabolic interactions, and networks involved in this subtype of glioma. *In vivo* longitudinal measurements of intratumoral 2HG levels will be highly valuable to probe target modulation in combination with pharmacokinetic/dynamic modeling of novel drugs acting on IDH-mutant glioma. We anticipate that it will prove critical to understand the complex and ongoing relationship between mutant IDH1 enzyme activity, 2HG levels, and tumor maintenance to successfully impact the course of this disease through targeted treatment or other selective agents such as metabolic inhibitors, demethylating agents, and synthetic lethality (20–22). Our measurements demonstrate the potential to probe pharmacologic modulation by *in vivo* 2HG measurements; however, at the moment, our study does not provide evidence for an early therapy termination based on the 2HG levels. Our methods are therefore expected to play an important role as precision medicine tools to accelerate clinical trials of *IDH* mutant–specific glioma therapies.

## Disclosure of Potential Conflicts of Interest

M.G. Vander Heiden has ownership interest (including patents) in and is a consultant/advisory board member for Agios Pharmaceuticals. T.T. Batchelor reports receiving commercial research grants from AstraZeneca and Pfizer; speakers bureau honoraria from Imedex, Merck, Oakstone Medical Publishing, Pharmawrite, and Research to Practice; and is a consultant/advisory board member for Accerta, Agenus, Amgen, Champions Biotechnology, Foundation Medicine, Kirin, Novartis, Proximagen, Roche, and Spectrum, UpToDate, Inc. No potential conflicts of interest were disclosed by the other authors.

## Authors' Contributions

**Conception and design:** O.C. Andronesi, F. Loebel, A.J. Iafrate, J. Dietrich, T.T. Batchelor, E.R. Gerstner, W.G. Kaelin, A.S. Chi, B.R. Rosen, D.P. Cahill
**Development of methodology:** O.C. Andronesi, F. Loebel, W. Bogner, M. Marjańska, B.R. Rosen
**Acquisition of data (provided animals, acquired and managed patients, provided facilities, etc.):** O.C. Andronesi, F. Loebel, A.J. Iafrate, J. Dietrich, T.T. Batchelor, E.R. Gerstner, B.R. Rosen, D.P. Cahill
**Analysis and interpretation of data (e.g., statistical analysis, biostatistics, computational analysis):** O.C. Andronesi, F. Loebel, A.J. Iafrate, E.R. Gerstner, A.S. Chi, B.R. Rosen, D.P. Cahill
**Writing, review, and/or revision of the manuscript:** O.C. Andronesi, F. Loebel, W. Bogner, M. Marjańska, M.G. Vander Heiden, A.J. Iafrate, J. Dietrich, T.T. Batchelor, E.R. Gerstner, A.S. Chi, B.R. Rosen, D.P. Cahill
**Administrative, technical, or material support (i.e., reporting or organizing data, constructing databases):** O.C. Andronesi, F. Loebel
**Study supervision:** O.C. Andronesi, D.P. Cahill

## Acknowledgments

The authors thank the technical support for developing 3D MRSI from Drs. Andre van der Kouwe, Borjan Gagoski, Aaron Hess, and Himanshu Bhat.

## Grant Support

This work was supported by NCI/NIH K22 Career Award 1K22CA178269-01 (to O.C. Andronesi); Burroughs-Wellcome Career Award, DFHCC/MIT Koch Institute Bridge Foundation and NIH Brain Cancer SPORE (to D.P. Cahill); NIH R01CA129371 and K24CA125440A (to T.T. Batchelor); Austrian Science Fund (FWF) KLI-61 (to W. Bogner); Biotechnology Research Center (BTRC) grant P41 RR008079 and P41 EB015894 (NIBIB), and NCC P30 NS057091 (M. Marjańska); NIH S10RR013026, S10RR021110, S10RR023401 (to B. Rosen).

The costs of publication of this article were defrayed in part by the payment of page charges. This article must therefore be hereby marked *advertisement* in accordance with 18 U.S.C. Section 1734 solely to indicate this fact.

Received March 20, 2015; revised September 15, 2015; accepted October 13, 2015; published OnlineFirst November 3, 2015.

## References

1. van den Bent MJ, Afra D, de Witte O, Ben Hassel M, Schraub S, Hoang-Xuan K, et al. Long-term efficacy of early versus delayed radiotherapy for low-grade astrocytoma and oligodendroglioma in adults: the EORTC 22845 randomised trial. Lancet 2005;366:985–90.
2. Shaw EG, Wang M, Coons SW, Brachman DG, Buckner JC, Stelzer KJ, et al. Randomized trial of radiation therapy plus procarbazine, lomustine, and vincristine chemotherapy for supratentorial adult low-grade glioma: initial results of RTOG 9802. J Clin Oncol 2012;30:3065–70.
3. Cairncross JG, Wang M, Jenkins RB, Shaw EG, Giannini C, Brachman DG, et al. Benefit from procarbazine, lomustine, and vincristine in oligodendroglial tumors is associated with mutation of IDH. J Clin Oncol 2014; 32:783–90.
4. Wen PY, Macdonald DR, Reardon DA, Cloughesy TF, Sorensen AG, Galanis E, et al. Updated response assessment criteria for high-grade gliomas: response assessment in neuro-oncology working group. J Clin Oncol 2010;28:1963–72.
5. van den Bent MJ, Wefel JS, Schiff D, Taphoorn MJ, Jaeckle K, Junck L, et al. Response assessment in neuro-oncology (a report of the RANO group): assessment of outcome in trials of diffuse low-grade gliomas. Lancet Oncol 2011;12:583–93.
6. Parsons DW, Jones S, Zhang XS, Lin JCH, Leary RJ, Angenendt P, et al. An integrated genomic analysis of human glioblastoma multiforme. Science 2008;321:1807–12.
7. Yan H, Parsons DW, Jin GL, McLendon R, Rasheed BA, Yuan WS, et al. IDH1 and IDH2 mutations in gliomas. N Engl J Med 2009;360:765–73.
8. Dang L, White DW, Gross S, Bennett BD, Bittinger MA, Driggers EM, et al. Cancer-associated IDH1 mutations produce 2-hydroxyglutarate. Nature 2009;462:739–44.
9. Xu W, Yang H, Liu Y, Yang Y, Wang P, Kim SH, et al. Oncometabolite 2-Hydroxyglutarate is a competitive inhibitor of alpha-ketoglutarate-dependent dioxygenases. Cancer Cell 2011;19:17–30.
10. Noushmehr H, Weisenberger DJ, Diefes K, Phillips HS, Pujara K, Berman BP, et al. Identification of a CpG island methylator phenotype that defines a distinct subgroup of glioma. Cancer Cell 2010;17:510–22.
11. Turcan S, Rohle D, Goenka A, Walsh LA, Fang F, Yilmaz E, et al. IDH1 mutation is sufficient to establish the glioma hypermethylator phenotype. Nature 2012;483:479–83.
12. Watanabe T, Nobusawa S, Kleihues P, Ohgaki H. IDH1 mutations are early events in the development of astrocytomas and oligodendrogliomas. Am J Pathol 2009;174:1149–53.
13. Kunz M, Thon N, Eigenbrod S, Hartmann C, Egensperger R, Herms J, et al. Hot spots in dynamic (FET)-F-18-PET delineate malignant tumor parts within suspected WHO grade II gliomas. Neuro Oncol 2011;13:307–16.
14. Andronesi OC, Kim GS, Gerstner E, Batchelor T, Tzika AA, Fantin VR, et al. Detection of 2-hydroxyglutarate in IDH-mutated glioma patients by *in vivo* spectral-editing and 2D correlation magnetic resonance spectroscopy. Sci Transl Med 2012;4:116ra4
15. Choi C, Ganji SK, DeBerardinis RJ, Hatanpaa KJ, Rakheja D, Kovacs Z, et al. 2-hydroxyglutarate detection by magnetic resonance spectroscopy in subjects with IDH-mutated gliomas. Nat Med 2012;18:624–9.

16. Pope WB, Prins RM, Thomas MA, Nagarajan R, Yen KE, Bittinger MA, et al. Non-invasive detection of 2-hydroxyglutarate and other metabolites in IDH1 mutant glioma patients using magnetic resonance spectroscopy. J Neuro Oncol 2012;107:197–205.
17. Elkhaled A, Jalbert LE, Phillips JJ, Yoshihara HAI, Parvataneni R, Srinivasan R, et al. Magnetic resonance of 2-hydroxyglutarate in IDH1-mutated low-grade gliomas. Sci Transl Med 2012;4:116ra5.
18. Kalinina J, Carroll A, Wang L, Yu Q, Mancheno DE, Wu S, et al. Detection of "oncometabolite" 2-hydroxyglutarate by magnetic resonance analysis as a biomarker of IDH1/2 mutations in glioma. J Mol Med 2012;90:1161–71.
19. Ward PS, Cross JR, Lu C, Weigert O, Abel-Wahab O, Levine RL, et al. Identification of additional IDH mutations associated with oncometabolite R(-)-2-hydroxyglutarate production. Oncogene 2012;31:2491–8.
20. Rohle D, Popovici-Muller J, Palaskas N, Turcan S, Grommes C, Campos C, et al. An inhibitor of mutant IDH1 delays growth and promotes differentiation of glioma cells. Science 2013;340:626–30.
21. Seltzer MJ, Bennett BD, Joshi AD, Gao P, Thomas AG, Ferraris DV, et al. Inhibition of glutaminase preferentially slows growth of glioma cells with mutant IDH1. Cancer Res 2010;70:8981–7.
22. Turcan S, Fabius AW, Borodovsky A, Pedraza A, Brennan C, Huse J, et al. Efficient induction of differentiation and growth inhibition in IDH1 mutant glioma cells by the DNMT inhibitor decitabine. Oncotarget 2013; 4:1729–36.
23. Murphy PS, Viviers L, Abson C, Rowland IJ, Brada M, Leach MO, et al. Monitoring temozolomide treatment of low-grade glioma with proton magnetic resonance spectroscopy. Br J Cancer 2004;90:781–6.
24. Guillevin R, Menuel C, Taillibert S, Capelle L, Costalat R, Abud L, et al. Predicting the outcome of grade II glioma treated with temozolomide using proton magnetic resonance spectroscopy. Br J Cancer 2011;104: 1854–61.
25. Bogner W, Gagoski B, Hess AT, Bhat H, Tisdall MD, van der Kouwe AJW, et al. 3D GABA imaging with real-time motion correction, shim update and reacquisition of adiabatic spiral MRSI. Neuroimage 2014;103:290–302.
26. Li S, Chou AP, Chen W, Chen R, Deng Y, Phillips HS, et al. Overexpression of isocitrate dehydrogenase mutant proteins renders glioma cells more sensitive to radiation. Neuro Oncol 2013;15:57–68.
27. Tran AN, Lai A, Li S, Pope WB, Teixeira S, Harris RJ, et al. Increased sensitivity to radiochemotherapy in IDH1 mutant glioblastoma as demonstrated by serial quantitative MR volumetry. Neuro Oncol 2014;16: 414–20.
28. Moffat BA, Chenevert TL, Lawrence TS, Meyer CR, Johnson TD, Dong Q, et al. Functional diffusion map: a noninvasive MRI biomarker for early stratification of clinical brain tumor response. Proc Natl Acad Sci U S A 2005;102:5524–9.
29. Ellingson BM, Cloughesy TF, Zaw T, Lai A, Nghiemphu PL, Harris R, et al. Functional diffusion maps (fDMs) evaluated before and after radiochemotherapy predict progression-free and overall survival in newly diagnosed glioblastoma. Neuro Oncol 2012;14:333–43.
30. van der Kouwe AJW, Benner T, Fischl B, Schmitt F, Salat DH, Harder M, et al. On-line automatic slice positioning for brain MR imaging. Neuroimage 2005;27:222–30.
31. Provencher SW. Estimation of metabolite concentrations from localized in-vivo proton NMR-spectra. Magn Reson Med 1993;30:672–9.
32. Reuter M, Rosas HD, Fischl B. Highly accurate inverse consistent registration: a robust approach. Neuroimage 2010;53:1181–96.
33. Ellingson BM, Malkin MG, Rand SD, Connelly JM, Quinsey C, LaViolette PS, et al. Validation of functional diffusion maps (fDMs) as a biomarker for human glioma cellularity. J Magn Reson Imaging 2010;31:538–48.
34. Capper D, Zentgraf H, Balss J, Hartmann C, von Deimling A. Monoclonal antibody specific for IDH1 R132H mutation. Acta Neuropathol 2009; 118:599–601.
35. Chi AS, Batchelor TT, Dias-Santagata D, Borger D, Stiles CD, Wang DL, et al. Prospective, high-throughput molecular profiling of human gliomas. J Neurooncol 2012;110:89–98.
36. Cairncross JG, Ueki K, Zlatescu MC, Lisle DK, Finkelstein DM, Hammond RR, et al. Specific genetic predictors of chemotherapeutic response and survival in patients with anaplastic oligodendrogliomas. J Natl Cancer Inst 1998;90:1473–9.
37. Hegi ME, Diserens A, Gorlia T, Hamou M, de Tribolet N, Weller M, et al. MGMT gene silencing and benefit from temozolomide in glioblastoma. N Engl J Med 2005;352:997–1003.
38. Yates JW, Chalmer B, McKegney FP. Evaluation of patients with advanced cancer using the Karnofsky performance status. Cancer 1980;45:2220–4.
39. Maudsley AA, Domenig C, Sheriff S. Reproducibility of serial whole-brain MR spectroscopic imaging. NMR Biomed 2010;23:251–6.
40. Bleeker FE, Atai NA, Lamba S, Jonker A, Rijkeboer D, Bosch KS, et al. The prognostic IDH1 (R132) mutation is associated with reduced NADP (+)-dependent IDH activity in glioblastoma. Acta Neuropathologica 2011;119:487–94.
41. Zinn PO, Sathyan P, Mahajan B, Bruyere J, Hegi M, Majumder S, et al. A novel volume-age-KPS (VAK) glioblastoma classification identifies a prognostic cognate microRNA-gene signature. PLoS One 2012;7: e41522.
42. van den Bent MJ, Brandes AA, Taphoorn MJ, Kros JM, Kouwenhoven MC, Delattre JY, et al. Adjuvant procarbazine, lomustine, and vincristine chemotherapy in newly diagnosed anaplastic oligodendroglioma: long-term follow-up of EORTC brain tumor group study 26951. J Clin Oncol 2013;31:344–50.
43. Chesnelong C, Chaumeil MM, Blough MD, Al-Najjar M, Stechishin OD, Chan JA, et al. Lactate dehydrogenase A silencing in IDH mutant gliomas. Neuro Oncol 2014;16:686–95.
44. Costalat R, Francoise JP, Menuel C, Lahutte M, Vallee JN, de Marco G, et al. Mathematical modeling of metabolism and hemodynamics. Acta Biotheor 2012;60:99–107.
45. Reitman ZJ, Jin GL, Karoly ED, Spasojevic I, Yang JA, Kinzler KW, et al. Profiling the effects of isocitrate dehydrogenase 1 and 2 mutations on the cellular metabolome. Proc Natl Acad Sci U S A 2011;108:3270–5.
46. Marin-Valencia I, Yang C, Mashimo T, Cho S, Baek H, Yang XL, et al. Analysis of tumor metabolism reveals mitochondrial glucose oxidation in genetically diverse human glioblastomas in the mouse brain *in vivo*. Cell Metab 2012;15:827–37.
47. Chaumeil MM, Larson PE, Woods SM, Cai L, Eriksson P, Robinson AE, et al. Hyperpolarized [1-13C] glutamate: a metabolic imaging biomarker of IDH1 mutational status in glioma. Cancer Res 2014;74:4247–57.
48. Beiko J, Suki D, Hess KR, Fox BD, Cheung V, Cabral M, et al. IDH1 mutant malignant astrocytomas are more amenable to surgical resection and have a survival benefit associated with maximal surgical resection. Neuro Oncol 2014;16:81–91.
49. Galldiks N, Rapp M, Stoffels G, Fink GR, Shah NJ, Coenen HH, et al. Response assessment of bevacizumab in patients with recurrent malignant glioma using [18F]Fluoroethyl-L-tyrosine PET in comparison to MRI. Eur J Nucl Med Mol Imaging 2013;40:22–33.
50. Carrillo JA, Lai A, Nghiemphu PL, Kim HJ, Phillips HS, Kharbanda S, et al. Relationship between tumor enhancement, edema, IDH1 mutational status, MGMT promoter methylation, and survival in glioblastoma. AJNR Am J Neuroradiol 2012;33:1349–55.